

# PHOTOCONDUCTION IN THE PEIERLS CONDUCTOR MONOCLINIC TaS<sub>3</sub>

V.E. Minakova<sup>a,\*</sup>, V.F. Nasretdinova<sup>a</sup>, S.V. Zaitsev-Zotov<sup>a,b</sup>

<sup>a</sup>Kotel'nikov Institute of Radio-engineering and Electronics of the RAS, 125009 Moscow, Russia

<sup>b</sup>Moscow Institute of Physics and Technology, 141700 Dolgoprudny, Russia

## Abstract

Photoconduction in the monoclinic phase of quasi-one-dimensional conductor TaS<sub>3</sub> has been observed at  $T < 70$  K. It was studied jointly with low-temperature ohmic and non-linear dark conduction. The strong sample quality dependence of both photoconduction and dark conduction at this temperature region has been observed. Together with a similarity of the main features of the photoconduction characteristic of both monoclinic ( $m$ -TaS<sub>3</sub>) and orthorhombic ( $o$ -TaS<sub>3</sub>) samples the following new peculiarities of photoconduction in  $m$ -TaS<sub>3</sub> were found: 1) the dependence of the activation energy of photoconduction on temperature,  $T$ , 2) the change of the recombination mechanism from the linear type to the collisional one at low  $T$  with a sample quality growth, 3) the existence of a fine structure of the electric-field dependence of photoconduction. Spectral study gives the Peierls energy gap value  $2\Delta^* = 0.18$  eV.

**Keywords:** Peierls conductors, charge-density wave, photoconduction, electron transport, collective transport

**PACS:** 71.45.Lr, 72.15.Nj, 71.20.Ps, 72.20.Jv, 73.20.Mf

## 1. Introduction

The specific properties of the Peierls conductors are due to charge-density-wave (CDW) formation accompanied by developing of the energy gap below the Peierls transition temperature  $T_P$  [1]. In such materials at small electric fields the CDW is pinned by impurities and defects. CDW sliding starts at the threshold field value  $E_T$  and leads to a strong non-linearity of I-V curves at  $E > E_T$ . At  $E'_T < E_T$  CDW creep is possible. It causes a weak non-linearity of I-V curve at  $E > E'_T$  which becomes clearly seen at low  $T$  [2]. At  $E < E'_T$  conductance is ohmic due to quasi-particles thermally exited over the Peierls gap.

Quasi-one-dimensional compound TaS<sub>3</sub> is known to have two crystal modifications, orthorhombic [3] and monoclinic [4].  $o$ -TaS<sub>3</sub> is one of the most studied Peierls conductors with a single Peierls transition at  $T_P \approx 220$  K and with completely gaped Fermi surface.

As a result, below  $T_P$  the temperature dependence of the ohmic conductance along the chain axis,  $G(T)$ , obeys an activation law with activation energy  $E_{\Delta\parallel} \approx 800$  K. It is known that  $G(T)$  begins to deviate from the initial activation law at  $T \lesssim T_P/2$ , a new activation energy being smaller [5], while the perpendicular conductance preserves the initial value  $E_{\Delta\perp} \approx 800$  K in all low-temperature range.  $G(T)$  curve shape at  $T \lesssim 100$  K is known to be highly dependent on sample quality – impurity contents and degrees of structural perfection. Sometimes even some plateau with weakly dependent conductance bridging between the regions with different activation parts of  $G(T)$  curve appears [6, 7, 8]. The origin of the longitudinal ohmic conduction change at low  $T$  observed both in different CDW materials (blue bronze, (TaSe<sub>4</sub>)<sub>2</sub>I) [1] and in spin-density-wave compounds [9] is still not fully understood. The observation and the study of photoconduction in  $o$ -TaS<sub>3</sub> [10, 11, 12] let us show that the main contribution into the low-temperature ohmic conduction is not due to quasi-particles exited over the Peierls gap, but mainly

\* e-mail: mina\_cplire@mail.ru

due to non-linear CDW excitations (such as solitons, excitons, dislocations *et al.*).

On the other hand, *m*-TaS<sub>3</sub> which undergoes two Peierls transitions at  $T_{P1} \approx 240$  K and  $T_{P2} \approx 160$  K is almost unstudied Peierls conductor. Since the first publication [4] there were only a few papers on this material later [6, 14, 15, 16, 17, 18]. So the data were very scarce and even the main transport properties of this compound especially at  $T < 77$  K were still unknown. For example, the first  $G(T)$  dependence presented in [4] was measured for a bundle of whiskers. The second one was obtained for a single crystal, but the main attention was paid to the high temperature region, only 10 points were measured at  $T < 77$  K. In [14]  $G(T)$  was studied only till 77 K. Non-linear conductance,  $G(E)$ , and  $G(T)$  studied in details at  $T < 77$  K in [6] were obtained for the only sample.  $G(T)$  obeyed an activation law without any change of value  $E_{\Delta} \approx 950$  K at all  $T$  down to 25 K in contrast with *o*-TaS<sub>3</sub> with a wide variety of  $G(T)$  curve shapes at this temperature region. In [16] there was just a mention that below 50 K both  $G(T)$  and  $G(E)$  become sample dependent,  $G(E)$  data were presented only at  $T \geq 66$  K. So a full picture of the conduction at  $T < 77$  K was absent. The photoconduction data were absent too. The main reason of a such data poverty is a complexity of reproducible *m*-TaS<sub>3</sub> synthesis. The aims of this work were to fill a missing data and to compare the results obtained with ones available for *o*-TaS<sub>3</sub> [6, 8, 12].

## 2. Experimental

*m*-TaS<sub>3</sub> crystals synthesized by the original technology combining the gradient technique with intermediate quenching were studied. The technology provides reproducible synthesis of *m*-TaS<sub>3</sub> with  $\approx 100$  % content of monoclinic phase crystals in the batch. Eight investigated samples from two batches were not so extremely thin as *o*-TaS<sub>3</sub> ones studied in [8, 10, 11, 12]. The typical transverse sample sizes were (1–10)  $\mu\text{m}$ . The measured heating effect was  $\lesssim 3$  mK due to excellent thermal contact with sapphire substrate.

Since both the dark conduction and photoconduction turned out to be highly dependent on a sample quality, we tried to use in our investigations *m*-TaS<sub>3</sub> samples of different quality in order to get a complete picture of the phenomenon. The quality was estimated in two ways: 1) by the measurement of electric-field dependent dark non-linear conductance at  $10 \text{ K} < T < 140 \text{ K}$  to determine  $E_T$  and  $E'_T$  values; 2) by the examination of dark ohmic conductance,  $G(T)$ , measured in a wide temperature range  $10 \text{ K} < T < 300 \text{ K}$  at sample voltage  $V \lesssim V'_T$ .

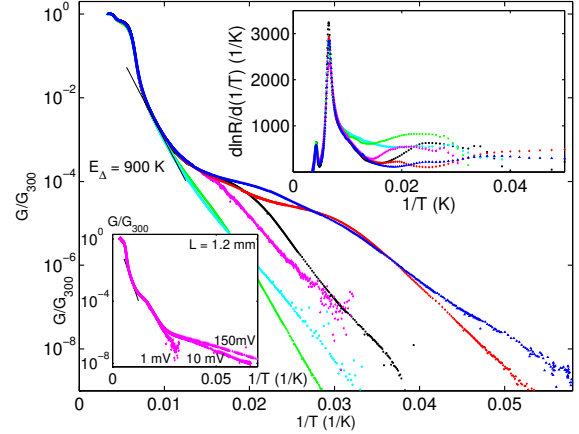


Figure 1: (Color online) Temperature dependences of dark ohmic conductance,  $G(T)$ , normalized to its room-temperature values,  $G_{300}$ , for different *m*-TaS<sub>3</sub> samples. Top inset shows corresponding temperature derivatives of the resistance,  $d \ln R / d(1/T)$ . Bottom inset shows  $G(T)$  curves measured at various sample voltages for the sample marked by magenta color in the main figure.

Three types of photoconduction study were undertaken. 1) Investigation of the temperature dependences of photoconductance,  $\delta G(T) = G(T, W) - G(T, 0)$ , at various light intensity levels,  $W$ , at  $V \lesssim V'_T$ . 2) Combined study of the electric-field dependences of non-linear dark conductance,  $G(E)$ , and of photoconductance,  $\delta G(E)$ , at different  $T$  and  $W$ . 3) Photoconduction spectroscopy for two types of the incident light polarization (along and transverse to the crystal chain axis) at photon energy range (0.1 – 0.45) eV at different  $T$ .

All conductance measurements were done along the chain direction in two-probe configuration in the voltage-controlled regime. A resistance of contacts made by indium cold soldering was  $\sim 10 \Omega$ . IR LED (light flux  $W = (10^{-4} - 30) \text{ mW/cm}^2$  at the sample position, a wavelength  $\lambda = 0.94 \mu\text{m}$ ) driven by meander-modulated current was used. The photon energy 1.3 eV was  $> 2\Delta^*$ . (For *o*-TaS<sub>3</sub>  $2\Delta^* = 0.25 \text{ eV}$  at  $T = 40 \text{ K}$  [13].) Photoconduction signal was measured by the usual AC modulation method at modulation frequency  $f = 4.5 \text{ Hz}$ . Photoconduction spectra were measured with a use of a grating monochromator (evacuated to a pressure below 1 Torr to reduce the effect of light absorption by the air) with a global,  $f = 3.125 \text{ Hz}$ . Other measurement details are in [8, 10, 11, 12, 19].

## 3. Temperature dependences of the ohmic conductance and of the photoconductance

Fig. 1 shows the dark  $G(T)$  dependences normalized to its room-temperature values,  $G_{300}$ , together with

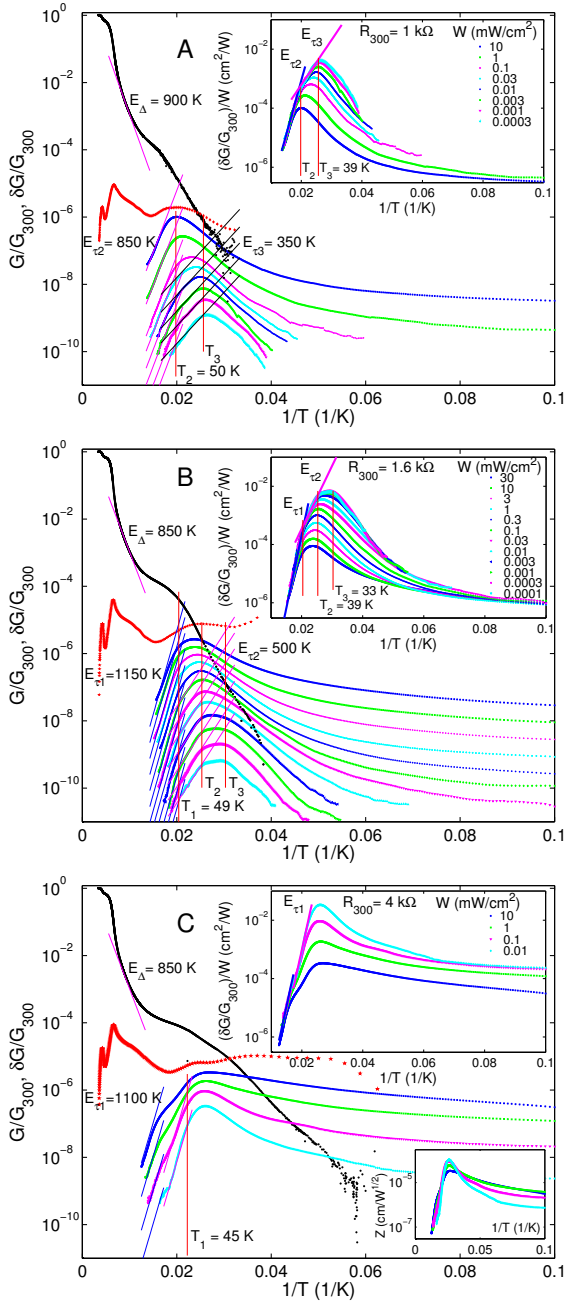


Figure 2: Sets of normalized temperature dependences of photoconductance,  $\delta G(T)/G_{300}$ , at different light intensities,  $W$ , together with normalized dependences of dark ohmic conductance,  $G(T)/G_{300}$ , (black curves) and temperature derivatives of the resistance,  $d \ln R/d(1/T)$ , (red curves, arb. units) for the samples of the groups A, B and C, respectively (see text). The top insets show the same dependences  $\delta G(T)/G_{300}$  normalized to corresponding values of  $W$ . The bottom inset shows the same dependences normalized to corresponding  $\sqrt{W}$  values:  $Z(T) = (\delta G(T)/G_{300})/\sqrt{W}$ .

corresponding temperature derivatives of the resistance,  $d \ln R/d(1/T)$ , (in the top inset) of  $m$ -TaS<sub>3</sub> samples. At  $T \gtrsim 77$  K the difference between the curves is small. For all the curves the well-defined activation region just below  $T_{P2}$  is absent, the activation energy  $E_{\Delta||} = 850 - 900$  K is temperature dependent,  $T_{P1} \approx 238$  K,  $T_{P2} \approx 153$  K. The situation changes at  $T \lesssim 77$  K: a huge difference of  $G(T)$  shapes analogous to one for  $o$ -TaS<sub>3</sub> appears. For low-quality samples a plateau in  $\log G(1/T)$  curve at  $T < 77$  K as a rule is small or is absent at all. With a sample quality growth the plateau width generally increases. A wide maximum is clearly seen in  $d \ln R/d(1/T)$  curve in this temperature region.

Six samples with different plateau width were chosen for the further investigations. To provide correct measurements of  $\delta G(T, W)$  amplitude both at the high and at the low temperature regions (where the signal is very small) the dependences  $\delta G(T)$  at all  $W$  were measured at both signs of the voltage bias for excluding LED current modulation crosstalk. The samples which were measured at the same conditions were divided into three groups (A, B and C, each of two samples) according with the shape of  $G(T)$  curve, see Fig. 2: small plateau width - A, large plateau width - B, huge plateau width - C. All figures below correspond to the same samples from the each group.

The common photoconduction features of  $m$ -TaS<sub>3</sub> and  $o$ -TaS<sub>3</sub> [8, 12] are the following:

- 1) Photoconduction is detected only at  $T \lesssim T_P/2$ .
- 2) The  $\delta G(T)$  dependences are non monotonic with a maximum, its magnitude and position,  $T_{max}$ , being dependent on  $W$ .
- 3) For the samples with a huge plateau region two maxima of  $\delta G(T)$  may take place (group C) [8].
- 4) There is a correlation between  $G(T)$  and  $\delta G(T)$ : for the samples with a wider plateau the  $G(T)$  value at a fixed  $T$  is larger, the  $\delta G/G_{300}$  signal at the maximum at fixed  $V$  and  $W$  values is larger too (group C, B). Moreover, both  $\delta G(T, W)$  maxima and a wide low-temperature  $d \ln R/d(1/T)$  maximum (red curve in Fig. 2) are approximately at the same  $T$ .  $T_{max}$  decreases with the plateau width growth,  $E_T$  value as a rule reduces too.

5)  $\delta G(W)$  dependence is linear at  $T > T_{max}$ . As a result,  $\delta G(T)$  curves at  $T > T_{max}$  obey the unique activation law for all  $W$ , the activation energy ( $E_{\tau 1}$  for groups B, C) being approximately the same for good-quality  $m$ -TaS<sub>3</sub> and  $o$ -TaS<sub>3</sub> samples. ( $E_{\tau}$  value is determined by the current carrier recombination time which obeys an activation law in this temperature region [8, 12].)

6) The activation energies in both materials are smaller for the low-quality samples ( $E_{\tau 2}$  for group B).

New photoconduction and dark ohmic conduction features of *m*-TaS<sub>3</sub> undetected in *o*-TaS<sub>3</sub> are observed:

1) There are several different temperature regions in the high temperature part of  $\delta G(T)$  curves (two regions for the group A samples and three regions for the group B ones) with different activation energies of  $\delta G(T)$ , the low-temperature activation energy being smaller. Unfortunately we have no data for the representative group C sample at sufficiently small  $W$  levels.

2) The region with the highest activation energy,  $E_{\tau 1}$ , is absent for the group A samples.

3) In these temperature regions a linear recombination regime takes place for all sample groups. As a result,  $\log \delta G(1/T)$  curves normalized to the corresponding  $W$  values coincide in the regions with different slopes, changing with  $T$  decrease (top insets in Fig. 2).

4) For the low-temperature region the recombination type is different for the different sample groups. For the low-quality samples  $\log \delta G(1/T)/W$  curves coincide also at  $T \lesssim 10$  K, indicating the linear type of recombination. The collisional recombination regime is not achieved for the group A samples at all available  $W$ . With a sample quality growth a region with a difference between these curves (near and just below  $T_{max}$ ) narrows,  $(\delta G/G_{300})/W$  value at low  $T$  becomes higher, and at last the difference between the curves at low  $T$  appears. For the group C (and for some of the group B) samples the linear recombination regime takes place at low  $T$  only for a small  $W$ . With  $W$  growth the situation changes: the coincidence of  $\delta G(T)$  curves normalized to corresponding  $\sqrt{W}$  values for large  $W$  at  $T \lesssim 30$  K (bottom inset in Fig. 2, C) indicates a transition into collisional recombination regime. So, we can conclude: the higher the sample quality is the smaller  $W$  values are required for the change of the recombination mechanism and for the realization of the collisional recombination regime at low  $T$ . This regime was also observed in pure *o*-TaS<sub>3</sub> samples at  $T \lesssim 30$  K [12].

5) For the samples with two maxima in  $\delta G(T)$  (group C) the plateau region in  $G(T)$  may split on two parts (Fig. 1, red curve), and the positions of  $d \ln R/d(1/T)$  curve peaks correlate with ones of  $\delta G(T)$  maxima.

6) The height of the low-temperature maximum in  $\delta G(T)$  may be both less and larger than the height of the high-temperature one.

#### 4. Electric-field dependences of the photoconduc-tance and of the dark conductance

Fig. 3 shows sets of normalized  $\delta G(E)$  curves collected at a fixed  $W$  (in the left) along with corresponding dark  $G(E)$  curves (in the right) at different  $T$  for the

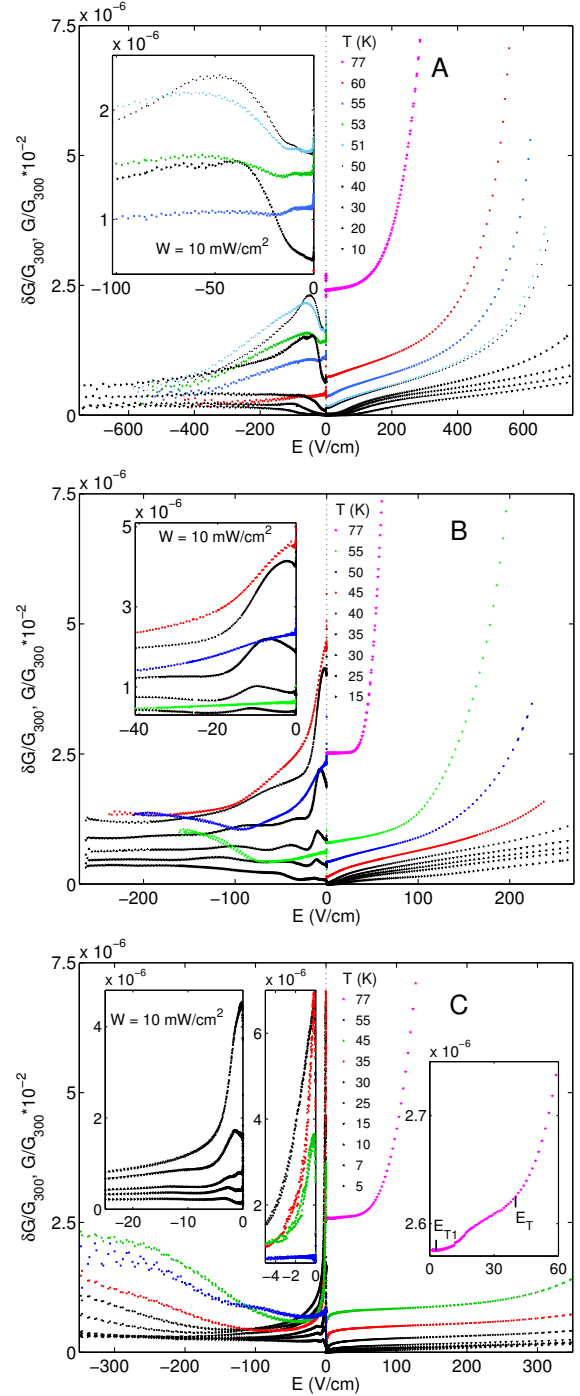


Figure 3: Sets of normalized electric-field dependences of the dark conductance,  $G(E)/G_{300}$ , (in the right) and of the corresponding normalized photoconductance,  $\delta G(E)/G_{300}$ , at a fixed  $W$  (in the left) for different  $T$  for all the sample groups. Color curves are measured at  $T > T_{max}$ , black ones – at  $T < T_{max}$ . Left and right insets show the initial parts of  $\delta G(E)$  and  $G(E)$  curves, respectively.

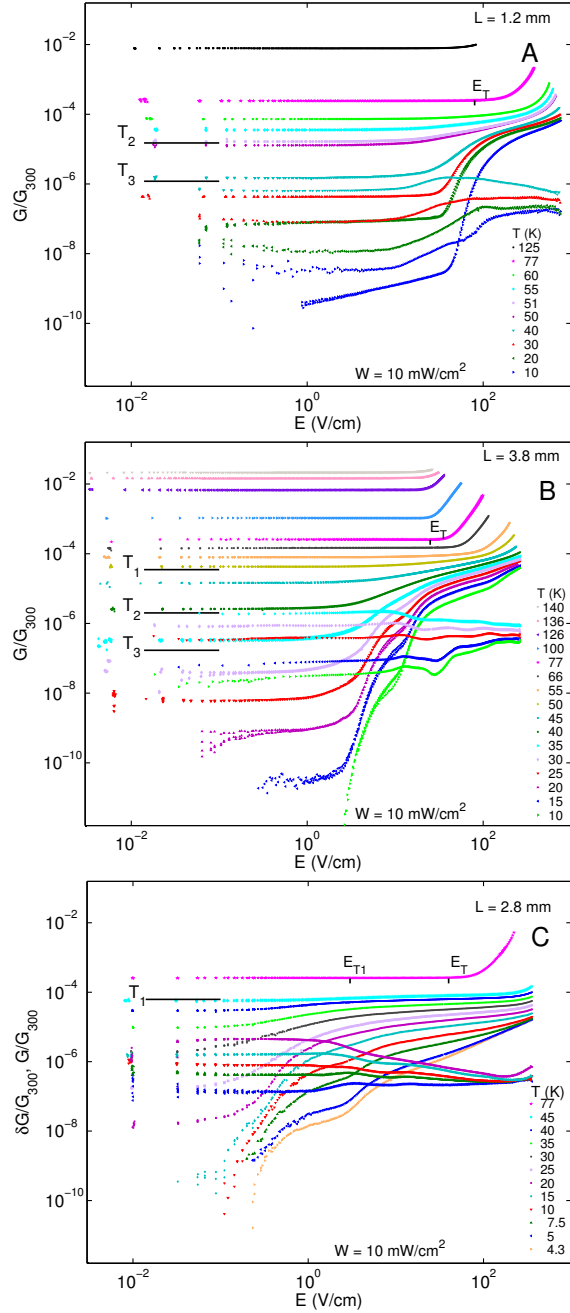


Figure 4: Normalized electric-field dependences of the dark conductance,  $G(E)/G_{300}$ , (upper set of data) and of the photoconductance,  $\delta G(E)/G_{300}$ , (lower set of data) at different  $T$  for all the sample groups.

all groups.  $G(E)$  measurements were made before the illumination to exclude residual photoconductance after turn-off of the light. All the curves were measured after application of voltage  $V > V_T$  to remove a metastability causing a strong hysteresis of the curves. Sample quality growth reduces the hysteresis. In Fig. 3 the color curves were measured at  $T > T_{max}$ , black ones – at  $T < T_{max}$ . Although the minimum of  $E_T$  value for our samples is achieved at  $T \approx 130 \text{ K}$ ,  $G(E)$  at  $T = 77 \text{ K}$  (magenta curves in Fig. 3, 4) are presented as a sample specification, the photoconductance is yet not seen.

The common features of photoconductance and dark conduction for all the sample groups are the following:

1) Both  $\delta G(E)$  and  $G(E)$  dependencies are highly non-linear.

2) The dark conductance decreases monotonously with a decrease of  $T$ .

3) The photoconductance change is non-monotonic with a decrease of  $T$ . Both an evolution and a shape of the color  $\delta G(E)$  curves in Fig. 3 differ from ones of the black curves. With a decrease of  $T$  the color  $\delta G(E)$  curves rise up and the peak at  $E = 0$  increases. With a further  $T$  decrease black  $\delta G(E)$  curves wholly come down, the peak splits and becomes smaller.

4) In whole, a  $\delta G(E)$  curve shape for all the groups is the similar. Almost for all  $T$  photoconductance decreases with an increase of  $E$  then for sufficiently large  $E$  values (group C, low  $T$  or all groups, high  $T$ ) it begins to growth. At  $T \lesssim 15 \text{ K}$  a growth of  $\delta G(E)$  is remarked.

The main differences of  $\delta G(E)$  and of  $G(E)$  dependences for various quality samples are the following:

1) The peak at  $E = 0$  dominates in  $\delta G(E)$  color curves for the samples of the groups B and C, whereas for the group A the peak at  $E = 0$  is of the same value or even less than neighbor one (left insets in Fig. 3).

2) The peak is higher and more narrow for more quality samples.

3) A fine structure of  $\delta G(E)$  dependences consisting of a few additional peaks develops with  $T$  decreasing. It is clearly seen at low  $T$  for groups B and C.

4) For group A the dependences  $G(E)$  are nonlinear at  $T \leq 77 \text{ K}$  for all  $E$ . Even at  $T = 77 \text{ K}$  a weak nonlinearity is preceded by the strong one. The abrupt threshold for the onset of CDW sliding is absent. A sufficiently sharp threshold for the group B sample and two-threshold behavior of  $G(E)$  curve (with  $E_{T1}$  and  $E_T$  values) for group C sample occur at  $T = 77 \text{ K}$ .

The sample difference is more clearly seen in Fig. 4, which shows the same sets of  $G(E)$  curves in a double logarithmic scale.  $E_T$  value of good-quality samples is a few times smaller than that of the group A.  $E_T$  increases with a decrease of  $T$  for all the groups. It is



difficult to determine distinctly the onset of a weak non-linearity,  $E'_T$ , at low  $T$  for all the samples. We can only say that  $E'_T$  value reduces with a decrease of  $T$  and becomes too small at low  $T$ . As a result, at  $E > E'_T$  an additional conduction channel turns on at  $T \lesssim 50$  K. Account of this fact is very important at  $G(T)$  measurements at low  $T$ . A small increase of a sample voltage leads to dramatic changes of  $G(T)$  shape: an additional  $G(T)$  curve deviation appears at low  $T$ , see bottom inset in Fig. 1 (group A sample). In this regime the low-temperature  $G(T)$  tail obeys an activation law, the activation energy being dependent on sample voltage. Such magenta curves measured at large voltages have a shape similar to ones for  $\sigma$ -TaS<sub>3</sub> samples in [6]. The fact that the same  $G(T)$  curve at  $V = 1$  mV does not change and has an activation behavior at least till  $T = 35$  K let us estimate the upper boundary of  $E'_T$  value for the group A sample at  $T = 35$  K. It is equal to 0.008 V/cm. Analogously,  $E'_T \leq 0.05$  V/cm at  $T = 30$  K for the group B,  $E'_T \leq 0.05$  V/cm at  $T = 20$  K for the group C. As it is known from the photoconduction study of  $\sigma$ -TaS<sub>3</sub> [10] the appearance of  $G(E)$  nonlinearity reduces the current carrier recombination time due to speed-up of recombination of spatially separated electrons and holes and leads to a decrease of photoconduction response.

Fig. 4 also helps to reveal invisible in Fig. 3 appearance and evolution of a fine structure of  $G(E)$  dependences with  $T$  decreasing, which is clearly seen for the groups B and C and is invisible for the group A.

Fig. 4 also shows  $\delta G(E)$  curves at low  $T$ . One can see some correlations between fine structures of  $\delta G(E)$  and  $G(E)$  curves: 1) the both types of fine structures exist in the same  $E$  and  $T$  regions, 2) the more explicitly the  $G(E)$  fine structure is seen the more visible the fine structure in  $\delta G(E)$  curves becomes. It seems the nature of the both fine structures is the same. Apparently,  $\delta G(E)$  fine structure may be also seen in  $\sigma$ -TaS<sub>3</sub>.

## 5. Photoconduction spectroscopy

Currently, photoconduction spectra were measured only for the samples of the groups A and B. The data obtained at  $T = 40$  K and voltage  $V = 500$  mV for both samples are shown in the Fig. 5, where  $S(\hbar\omega) = \delta G/\hbar\omega$ . The spectra shape reminds that of  $\sigma$ -TaS<sub>3</sub> [13, 19] except for a wide peak at 0.15 eV. The data look more reproducible than those in  $\sigma$ -TaS<sub>3</sub> except for an additional step-like structure (periodical oscillations with  $\approx 50$  meV periodicity) seen on the group B sample data. The measured Peierls energy gap value,  $2\Delta^* = 0.18$  eV.

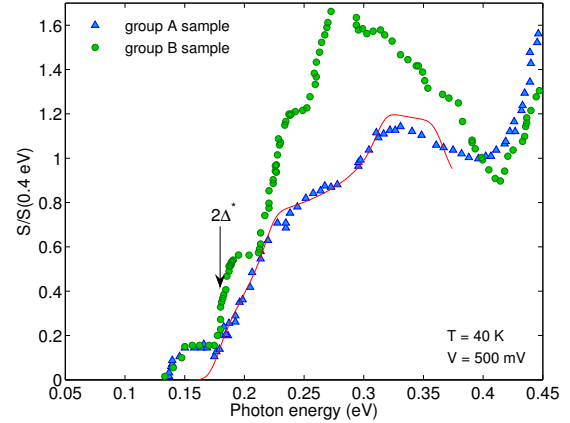


Figure 5: Photoconduction spectra of the samples of the groups A and B. Solid curve shows the best fitting by the Peierls gap modulation model [13].

## 6. Concluding remarks

The studied  $m$ -TaS<sub>3</sub> samples have been divided into three groups depending on plateau width in  $G(T)$  curve. The samples sizes were approximately the same. The experimental conditions were also the same for all the samples. All the measured dependences for these groups turned out to be different. So, the reason of the difference between all the sample groups is mainly the sample quality, which is determined by two factors: 1) impurity contents, 2) degrees of structural perfection.

The impurity contents were different: the low-quality samples ( $E_T > 25$  V/cm) – group A and good-quality samples ( $E_T = 3 - 15$  V/cm) – groups B and C. Unfortunately we had no high-quality samples ( $E_T \lesssim 1$  V/cm). So the group A samples differ from the group B and C ones firstly due to impurity contents. The presence of impurities kills all fine effects – the fine structure of  $G(E)$  and  $\delta G(E)$ , step-like structure of the spectrum, high temperature part of  $\delta G(T)$  curve characterizing by the highest activation energy value,  $E_{T1}$ . Thus the presence of impurities reduces the current carrier recombination time due to providing an additional channel of non-equilibrium current carrier recombination and leads to an impossibility of the realization of the collisional recombination regime at low  $T$ .

As a rule, the plateau width is smaller for the low-quality samples both for  $\sigma$ -TaS<sub>3</sub> and  $m$ -TaS<sub>3</sub> case. But the presence of impurities is not the only reason of the plateau reduction. For example, we have met  $\sigma$ -TaS<sub>3</sub> samples doped by Nb (concentration  $\sim 0.5\%$ ) with a huge plateau. In our opinion the additional reason of the difference between the groups is due to different degrees

of structural perfection, which we unfortunately can not control. It seems a big plateau is caused by a structural inhomogeneity of the crystal. Two different types of the inhomogeneity (which we can not distinguish yet) may take place. 1) A sample may be an aggregate of a few parallel crystals with different  $E_T$  values (the longitudinal stripe structure is often seen in thick *o*-TaS<sub>3</sub> crystals). 2) A sample may be deformed by outside factors – for example by stretch arising in the process of contacts fabrication. Our preliminary results obtained for *o*-TaS<sub>3</sub> crystals with different degrees of the longitudinal stretch confirm this assumption. It seems impurities prevent a sample from outside deformation, it leads to the reduction of the stretch possibility of the low-quality samples.

It also worth to mention that  $G(E)$  dependencies of our samples in general are consistent with the same ones for high quality *m*-TaS<sub>3</sub> sample reported in [6]. Moreover the same fine structure is also present but was not remarked and discussed in [6]. The similar peculiarities of IV-curves were also observed and analyzed in impure samples of *o*-TaS<sub>3</sub> at  $T \lesssim 10$  K [20] where they were attributed to the difference of the pinning potentials provided by various impurities. Here such a difference may also come from separate depinning of two CDWs.

Another interesting observation is very strong and unusual  $\delta G(E)$  dependence. The concurrence of two physical mechanisms may result in such a complex behavior. On the one hand, spatial separation of electrons and holes caused by fluctuations of the chemical potential (which are significant at low  $T$  [21]) complicates their recombination process [10, 11]. However the process accelerates with CDW motion. On the other hand, with a decrease of  $T$  a role of electric-field dependent electronic states with relatively small excitation energies (impurities, defects, excitons *et al.*) which can promote the non-equilibrium current carrier recombination increases. Our photoconduction spectroscopy data confirm the existence of the electric-field dependent electronic states in *o*-TaS<sub>3</sub> [19].

The group A spectrum shape can be reasonably fitted (solid curve in Fig. 5) within a simple model of Peierls gap modulation [13] except for a small and wide peak around 0.15 eV. This spectrum exhibits van Hove singularities arising due to the manifestation of the 3D properties of the compound. The detail discussion of the origin of van Hove singularities in both *o*-TaS<sub>3</sub> and *m*-TaS<sub>3</sub> case one can find in [13]. Surprisingly, no signature of the second Peierls gap is seen at  $\hbar\omega < 0.4$  eV. The group B spectrum shape is very similar but complicated by an additional periodical step-like structure. The period of these oscillations ( $\approx 50$  meV) is too big to be attributed to the light interference, so it is more likely corresponds

to the phonon repetitions of the peak 0.15 eV. Similar oscillatory structure has been also found in *o*-TaS<sub>3</sub>.

The main results of photoconduction and of low-temperature conduction study in Peierls conductor *m*-TaS<sub>3</sub> are similar to ones in *o*-TaS<sub>3</sub>. However much more details are observed in *m*-TaS<sub>3</sub>. The differences are believed to be a consequence of more perfect crystal structure of *m*-TaS<sub>3</sub> in comparison with *o*-TaS<sub>3</sub>. For example, it is known that the RF-field response in *m*-TaS<sub>3</sub> also is more pronounced than that in *o*-TaS<sub>3</sub> due to more higher CDW coherence in monoclinic phase of the compound [18]. So, *m*-TaS<sub>3</sub> is very grace object of research. The obtained phenomenon picture is very complex and needs further investigations, which as we hope let us clarify the nature of low-temperature conduction in CDW materials.

**Acknowledgements.** The work was supported by RFBR project 14-02-01236 and Department of physical science of RAS.

## References

- [1] As a review: P. Monceau, *Adv. Phys.* **61** (2012) 325; G. Grüner, *Rev. Mod. Phys.* **60** (1988) 1129.
- [2] S. V. Zaitsev-Zotov, *Phys. Rev. Lett.*, **71** (1993) 605.
- [3] E. Bjerkelund, A. Kjekshus, *Z. Anorg. Allgem. Chem.* **328**, 235 (1964); E. Bjerkelund, J. H. Fermor, A. Kjekshus, *Acta Chem. Scand.* **20** (1966) 1836.
- [4] A. Meerschaut, J. Rouxel, P. Haen, P. Monceau, M. Núñez-Regueiro, *J. Phys.* **40** (1979) L-157.
- [5] T. Takosima *et al.*, *Sol. State Commun.* **35** (1980) 911.
- [6] M. E. Itkis, F. Ya. Nad', P. Monceau, *J. Phys.: Condens. Matter* **2** (1990) 8327.
- [7] D. Starešinić *et al.*, *Phys. Rev. B.*, **65** (2002) 165109.
- [8] S. V. Zaitsev-Zotov, V. E. Minakova, V. F. Nasretidinova, S. G. Zybtshev, *Physica B* **407** (2012) 1868.
- [9] G. Grüner, *Rev. Mod. Phys.* **66** (1994) 1.
- [10] S. V. Zaitsev-Zotov, V. E. Minakova, *JETP Lett.*, **79** (2004) 550.
- [11] S. V. Zaitsev-Zotov, V. E. Minakova, *J. Phys. IV France*, **131** (2005) 95.
- [12] S. V. Zaitsev-Zotov, V. E. Minakova, *Phys. Rev. Lett.*, **97** (2006) 266404.
- [13] S. V. Zaitsev-Zotov, V. F. Nasretidinova, V. E. Minakova, present volume.
- [14] A. Meerschaut, L. Guemas, J. Rouxel, *C. R. Acad. Sci (France)* (1980) C-215.
- [15] C. Roucau *et al.*, *Phys. Status Solidi (a)* **62** (1980) 483.
- [16] K. Hasegawa, A. Maeda, S. Uchida, S. Tanaka, *Sol. State Commun.*, **44** (1982) 881.
- [17] A. Maeda, M. Naito, S. Tanaka, *J. Phys. Soc. Jap.*, **54** (1985) 1912.
- [18] Yu. I. Latyshev, V. E. Minakova, *Physica B+C* **143** (1986) 155.
- [19] V. F. Nasretidinova, S. V. Zaitsev-Zotov, *JETP Lett.*, **89** (2009) 514.
- [20] S. V. Zaitsev-Zotov, G. Remenyi, P. Monceau, *Phys. Rev. Lett.*, **78** (1997) 1098.
- [21] V. Ya. Pokrovskii, S. V. Zaitsev-Zotov, *Synth. Metals*, **32** (1989) 321.